

Optimal training of variational quantum algorithms without barren plateaus

Tobias Haug^{1,*} and M. S. Kim¹

¹QOLS, Blackett Laboratory, Imperial College London SW7 2AZ, UK

Variational quantum algorithms (VQAs) promise efficient use of near-term quantum computers. However, training VQAs often requires an extensive amount of time and suffers from the barren plateau problem where the magnitude of the gradients vanishes with increasing number of qubits. Here, we show how to optimally train a VQA for learning quantum states. Parameterized quantum circuits can form Gaussian kernels, which we use to derive optimal adaptive learning rates for gradient ascent. We introduce the generalized quantum natural gradient that features stability and optimized movement in parameter space. Both methods together outperform other optimization routines and can enhance VQAs as well as quantum control techniques. The gradients of the VQA do not vanish when the fidelity between the initial state and the state to be learned is bounded from below. We identify a VQA for quantum simulation with such a constraint that thus can be trained free of barren plateaus. Finally, we propose the application of Gaussian kernels for quantum machine learning.

Quantum computers promise to tackle important problems that can be difficult for classical computers. To effectively use quantum computers available in the near future [1, 2] variational quantum algorithms (VQAs) have been put forward. These VQAs solve tasks by iteratively updating a parameterized quantum circuit (PQC) with a classical optimization routine in a feedback loop [3–6]. However, training of such VQAs can take an extensive amount of iterations, yielding a long time until the algorithm converges. Further, VQAs are often impeded by the barren plateau problem where the variance of the gradients vanish exponentially with increasing number of qubits [7], specific cost functions [8], entanglement [9] and noise [10]. Further, the optimization routine of VQAs was shown to be NP-hard even for problems that are easy for classical computers [11]. Quantum algorithms that can avoid training PQCs to circumvent the barren plateau problem have been proposed [12–17]. To improve training of VQAs, one can use quantum geometric information to define the quantum natural gradient (QNG) [18–20]. However, the QNG can be unstable without regularization [21–23] and suffers from barren plateaus as well [24]. Further, the learning rates for training with the QNG are so far chosen only in a heuristic manner. With these challenges in mind, an important task for quantum computers is learning quantum states. Here, the PQC is trained to represent a given quantum state. Besides the importance for state preparation, this core routine is encountered in many VQAs, such as the projected variational quantum dynamics method [25, 26], variational fast forwarding [27], learning of scramblers [28], quantum circuit born machines [29], quantum generative adversarial networks [30], quantum autoencoders [31] and excited state calculations [32].

Here, we show how to optimally train a VQA to represent quantum states. We find that the fidelity between two states forms an approximate Gaussian kernel in respect to the distance in parameter space of the PQC,

with the quantum Fisher information metric (QFIM) as the weight matrix. With this result, we derive the optimal adaptive learning rate for gradient ascent. Further, we introduce the generalized quantum natural gradient (GQNG) that interpolates between standard gradient and QNG. We find a type of GQNG that is stable without regularization while providing good movement in parameter space. For learning quantum states using the fidelity, adaptive learning rates and QNG combined outperform other optimization techniques. We analytically derive the variance of the gradient of the VQA. Under the condition that the fidelity between the initial state and the state to be learned has a lower bound, the variance of the gradient has a lower bound that is independent of the number of qubits. Thus, the gradient will not vanish with increasing number of qubits. We show a type of VQA, the projected variational quantum dynamics method or restarted quantum dynamics method [25, 26], that fulfills this condition and thus can be trained free of barren plateaus. Our methods can improve various VQAs and numerical quantum control techniques, and promise implementation on near-term quantum computers. As further application, our results are directly relevant for quantum machine learning. The Gaussian kernel can be realized by hardware-efficient PQCs to run quantum machine learning algorithms on the current quantum hardware.

Model— A unitary $U(\boldsymbol{\theta})$ parameterized by the M -dimensional parameter vector $\boldsymbol{\theta} \in \mathbb{R}^M$ generates the quantum state $|\psi(\boldsymbol{\theta})\rangle = U(\boldsymbol{\theta})|0\rangle$ consisting of N qubits (see Fig.1a). Our goal is to learn the target parameters $\boldsymbol{\theta}_t$ that approximate a given target state $|\psi_t\rangle$ (see Fig.1b). This is achieved by the optimization task $\boldsymbol{\theta}_t = \text{argmax}_{\boldsymbol{\theta}} K_t(\boldsymbol{\theta})$, where $K_t(\boldsymbol{\theta}) = |\langle\psi_t|\psi(\boldsymbol{\theta})\rangle|^2$ is the fidelity. A common approach to optimize the fidelity is standard gradient ascent. Here, one calculates the gradient of the fidelity $\nabla K_t(\boldsymbol{\theta})$, which is the direction of largest increase for the fidelity. Then, the parameter $\boldsymbol{\theta}$ is iteratively updated with the rule $\boldsymbol{\theta}' = \boldsymbol{\theta} + \alpha \nabla K_t(\boldsymbol{\theta})$,

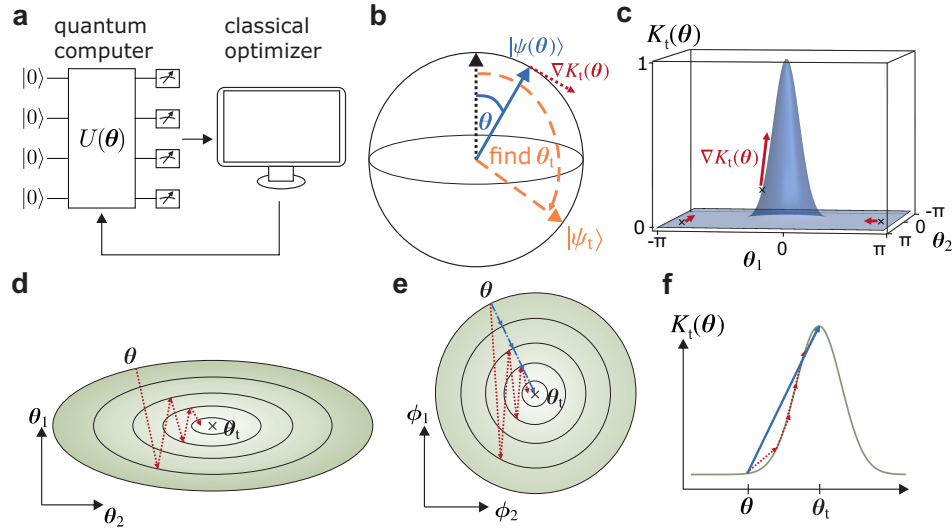


FIG. 1. **a)** The variational quantum algorithm (VQA) consists of a parameterized quantum circuit (PQC) that generates the quantum state $|\psi(\theta)\rangle = U(\theta)|0\rangle$ with unitary $U(\theta)$ and parameters θ , as well as a classical optimization routine. Measurements on the quantum state are used to calculate the cost function, which is then optimized by the classical optimizer in a feed back loop by adjusting the parameters θ . **b)** VQA to represent the target state $|\psi_t\rangle$ using $|\psi(\theta)\rangle$. Goal is to find target parameters $\theta_t = \operatorname{argmax}_{\theta} K_t(\theta)$ that approximate the target state by maximizing the fidelity $K_t(\theta) = |\langle\psi_t|\psi(\theta)\rangle|^2$. Training is performed using the gradient $G_0(\theta) = \nabla K_t(\theta)$, which points in the direction of steepest increase of fidelity. **c)** The landscape of the fidelity $K_t(\theta)$ as function of θ often have barren plateaus, where the fidelity and its gradients are exponentially small within most of the parameter space. However, as long as the initial quantum state of the VQA is guaranteed to have a lower bounded fidelity, then the magnitude of the gradient does not vanish even for many qubits and barren plateaus can be avoided (Eq. 11). **d)** Gradient ascent optimises the fidelity by updating $\theta' = \theta + \alpha G_0(\theta)$. As the fidelity landscape as function of θ is in general not euclidean, standard gradient ascent does not take the fastest path. **e)** By using quantum geometric information about the parameter space with the quantum Fisher information metric (QFIM) $\mathcal{F}(\theta)$, the parameter space can be transformed to get the quantum natural gradient (QNG) which moves in the optimal direction (see solid blue curve). To yield stable gradients in practice, the QNG requires regularization. The generalized quantum natural gradient (GQNG) (Eq. (5)) interpolates between standard gradient and QNG, and can be stable without regularization. **f)** The step size α for the gradient update is normally a fixed heuristic learning rate (dashed red curves). The fidelity of PQCs can form Gaussian kernels, which is used to calculate the optimal adaptive learning rate (Eq. (8)) for each gradient update (blue solid curve).

where α is the learning rate. After a number of iterations, the quality of the found approximate solution θ'_t is measured with the infidelity

$$\Delta K_t(\theta'_t) = 1 - K_t(\theta'_t) = 1 - |\langle\psi_t|\psi(\theta'_t)\rangle|^2. \quad (1)$$

However, training VQAs is plagued by the following issues. First, the gradient often becomes exponentially small with increasing number of qubits due to the barren plateau problem (see Fig. 1c). Second, the update rule assumes that the parameter space is euclidean, i.e. the fidelity varies at the same rate for every parameter direction. However, in general this is not the case as seen in Fig. 1d. Then, the standard gradient is not the optimal direction for the parameter update. This can be aided by using the QFIM $\mathcal{F}(\theta)$. For $|\psi\rangle = |\psi(\theta)\rangle$, it is given by [33]

$$\mathcal{F}_{ij}(\theta) = 4[\langle\partial_i\psi|\partial_j\psi\rangle - \langle\partial_i\psi|\psi\rangle\langle\psi|\partial_j\psi\rangle], \quad (2)$$

where $\partial_j|\psi\rangle$ is the gradient in respect to the j -th element of θ . For pure states, the QFIM tells us the change of

fidelity for small parameter variations $d\mu$ [24, 33, 34]

$$\mathcal{K}(\theta, \theta + d\mu) = |\langle\psi(\theta)|\psi(\theta + d\mu)\rangle|^2 = 1 - \frac{1}{4}d\mu^T \mathcal{F}(\theta) d\mu. \quad (3)$$

The QFIM contains information about how the geometry of the parameter space is related to the geometry of quantum states. The QNG $G_1(\theta) = \mathcal{F}^{-1}(\theta)\nabla K_t(\theta)$ [18–20] utilizes this information to construct gradient updates which move optimally in the parameter space (see Fig. 1e). However, when applied in practice the QNG requires an additional hyperparameter for regularization to take care of the ill-conditioned inverse of the QFIM [21–23]. Third, the learning rate α is generally not known and is often determined only heuristically by setting it to a small constant (see Fig. 1f). In the following, we show how to optimally perform gradient ascent by using the QNG and adaptive learning rates, as well as the conditions to avoid barren plateaus.

We propose that the fidelity as a function of parameter θ can be approximated as a Gaussian kernel. In particular, we have two quantum states of the PQC $|\psi(\theta)\rangle$ and

$|\psi(\boldsymbol{\theta}')\rangle$ with parameters $\boldsymbol{\theta}, \boldsymbol{\theta}'$ and a distance in parameter space $\Delta\boldsymbol{\theta} = \boldsymbol{\theta} - \boldsymbol{\theta}'$. Then, the fidelity is given by

$$\mathcal{K}(\boldsymbol{\theta}, \boldsymbol{\theta}') = |\langle\psi(\boldsymbol{\theta})|\psi(\boldsymbol{\theta}')\rangle|^2 \approx \exp\left[-\frac{1}{4}\Delta\boldsymbol{\theta}^T \mathcal{F}(\boldsymbol{\theta}) \Delta\boldsymbol{\theta}\right], \quad (4)$$

where this approximation is valid within a distance $|\Delta\boldsymbol{\theta}| < \epsilon_G$ with $\epsilon_G > 0$. Here, the QFIM $\mathcal{F}(\boldsymbol{\theta})$ plays the role of the weight matrix of the kernel. The first order approximation $\mathcal{K}(\boldsymbol{\theta}, \boldsymbol{\theta}') \approx 1 - \frac{1}{4}\Delta\boldsymbol{\theta}^T \mathcal{F}(\boldsymbol{\theta}) \Delta\boldsymbol{\theta}$ returns Eq. (3) as expected [33, 34]. We show an exactly solvable PQC with Gaussian kernel in the Supplemental Materials. In Fig. 2a, we find that various types of expressive PQCs match well with the Gaussian kernel, which improves with increasing number of qubits. We note that for large parameter norm $\Delta\boldsymbol{\theta}^T \mathcal{F}(\boldsymbol{\theta}) \Delta\boldsymbol{\theta}$ the fidelity deviates from Eq. (4) and eventually reaches the constant value $\langle\mathcal{K}_{\text{rand}}\rangle = \frac{1}{2^N}$ given by effectively random states [7, 35]. We can use this result to derive an upper bound for ϵ_G . Assuming a simple QFIM $\mathcal{F} = \frac{I}{b}$ with I being the identity and $b > 0$ some constant, we find $\epsilon_G < 2\sqrt{bN \log(2)}$.

We now replace the standard gradient $\nabla K_t(\boldsymbol{\theta})$ in gradient ascent with the GQNG

$$G_\beta(\boldsymbol{\theta}) = \mathcal{F}^{-\beta}(\boldsymbol{\theta}) \nabla K_t(\boldsymbol{\theta}), \quad (5)$$

where $\beta \in [0, 1]$. As special cases, we have the standard gradient for $G_0(\boldsymbol{\theta}) = \nabla K_t(\boldsymbol{\theta})$ and the QNG for $G_1(\boldsymbol{\theta}) = \mathcal{F}^{-1}(\boldsymbol{\theta}) \nabla K_t(\boldsymbol{\theta})$ [18, 20]. The inverse of the QFIM $\mathcal{F}^{-1}(\boldsymbol{\theta})$ is highly sensitive to small changes in parameter $\boldsymbol{\theta}$ as often $\mathcal{F}(\boldsymbol{\theta})$ is ill conditioned due to small eigenvalues of the QFIM. This causes the QNG to become unstable and gradient ascent cannot converge. A common approach to regularize the QNG is by adding the identity matrix to the QFIM before inversion $\mathcal{F}' = \mathcal{F} + \epsilon_R I$, where I is the identity matrix and ϵ_R is a small hyperparameter. This hyperparameter has to be determined heuristically and may depend on the particular QFIM [21–23]. We now show when regularization $\epsilon_R > 0$ is necessary for the GQNG. For arbitrary β and $\epsilon_R = 0$, the fidelity after one gradient ascent update step $\boldsymbol{\theta}' = \boldsymbol{\theta} + \alpha G_\beta(\boldsymbol{\theta})$ with arbitrary learning rate α is given by (derivation in Supplemental materials)

$$K_t(\boldsymbol{\theta}') = K_t(\boldsymbol{\theta}) \exp\left[-\frac{1}{4}(\alpha^2 \nabla K_t^T(\boldsymbol{\theta}) \mathcal{F}^{1-2\beta}(\boldsymbol{\theta}) \nabla K_t(\boldsymbol{\theta}) + 2\alpha \Delta\boldsymbol{\theta}^T \mathcal{F}^{1-\beta}(\boldsymbol{\theta}) \nabla K_t(\boldsymbol{\theta}))\right]. \quad (6)$$

For $\beta > \frac{1}{2}$, Eq. 6 contains the QFIM with negative exponent $\mathcal{F}^{1-2\beta}$. In this case, an ill-conditioned QFIM can lead to an excessively large parameter update that moves us away from the target parameters instead of bringing us closer. Here, the QFIM has to be regularized with a parameter $\epsilon_R > 0$ in order to ensure that it is not ill-conditioned. For $\beta \leq \frac{1}{2}$ the QFIM appears only with non-negative exponents in Eq. 6. Even if the QFIM is

ill-conditioned, the updated fidelity is not affected by it. Thus, the GQNG with $\beta = \frac{1}{2}$ and $G_{\frac{1}{2}}(\boldsymbol{\theta}) = \mathcal{F}^{-\frac{1}{2}} \nabla K_t(\boldsymbol{\theta})$ is intrinsically stable without the need of further regularization and we can set $\epsilon_R = 0$.

Next, we show the optimal adaptive learning rates for gradient ascent (derivation in Supplemental materials). The initial update rule is given by $\boldsymbol{\theta}_1 = \boldsymbol{\theta} + \alpha_1 G_\beta(\boldsymbol{\theta})$ with the learning rate

$$\alpha_1 = \frac{2\sqrt{-\log(K_t(\boldsymbol{\theta}))}}{\sqrt{G_\beta(\boldsymbol{\theta})^T \mathcal{F}(\boldsymbol{\theta}) G_\beta(\boldsymbol{\theta})}}. \quad (7)$$

If the PQC is unable to represent the target state perfectly, i.e. $\max_{\boldsymbol{\theta}} |\langle\psi(\boldsymbol{\theta})|\psi_t\rangle|^2 = K_0 < 1$, where K_0 is the maximal possible fidelity, we can adjust the step using $K_t(\boldsymbol{\theta}_1)$. Then, the updated parameter $\boldsymbol{\theta}'_t$ is given by $\boldsymbol{\theta}'_t = \boldsymbol{\theta} + \alpha_t G_\beta(\boldsymbol{\theta})$ with the adaptive learning rate

$$\alpha_t = \frac{1}{2} \left(\frac{4}{\alpha_1 G_\beta(\boldsymbol{\theta}) \mathcal{F}(\boldsymbol{\theta}) G_\beta(\boldsymbol{\theta})} \log\left(\frac{K_t(\boldsymbol{\theta}_1)}{K_t(\boldsymbol{\theta})}\right) + \alpha_1 \right). \quad (8)$$

This concludes one step of adaptive gradient ascent. By setting $\boldsymbol{\theta} = \boldsymbol{\theta}'_t$ and repeating above steps, the next iteration of adaptive gradient ascent is performed.

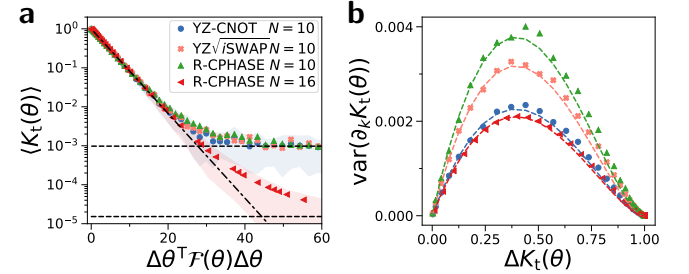


FIG. 2. a) Average fidelity $\langle K_t(\boldsymbol{\theta}) \rangle$ as function of parameter norm $\Delta\boldsymbol{\theta}^T \mathcal{F}(\boldsymbol{\theta}) \Delta\boldsymbol{\theta}$, with distance $\Delta\boldsymbol{\theta} = \boldsymbol{\theta} - \boldsymbol{\theta}_t$ and target parameters $\boldsymbol{\theta}_t$. Shaded area is the 20-th and 80-th percentile of the fidelity. We find a good match with the Gaussian kernel (Eq. 4, dash-dotted line). For large norm, we see the fidelity converges to the fidelity given by random states $\langle\mathcal{K}_{\text{rand}}\rangle = \frac{1}{2^N}$ (dashed lines). We use three different PQCs with randomized parameters, which are defined in the Supplemental materials. Number of layers $p = 20$ for R-CPHASE $N = 10$, $p = 16$ for $N = 16$, else $p = 10$. Average over 50 random instances of $\boldsymbol{\theta}_t$. b) Variance of gradient $\text{var}(\partial_k K_t(\boldsymbol{\theta}))$ against infidelity $\Delta K_t(\boldsymbol{\theta})$ for different types of PQCs. Dashed lines are the analytic formula Eq. (9) for the variance.

For a given fidelity $K_t(\boldsymbol{\theta})$, we can derive the variance of the gradient analytically (see Supplemental materials)

$$\begin{aligned} \text{var}(\partial_k K_t(\boldsymbol{\theta})) &= \langle\langle (\partial_k K_t(\boldsymbol{\theta}))^2 \rangle\rangle_{\Delta\boldsymbol{\theta}} - \langle\langle \partial_k K_t(\boldsymbol{\theta}) \rangle\rangle_{\boldsymbol{\theta}}^2 \\ &= \frac{1}{M} \frac{\text{Tr}(\mathcal{F}(\boldsymbol{\theta})^2)}{\text{Tr}(\mathcal{F}(\boldsymbol{\theta}))} K_t(\boldsymbol{\theta})^2 \log\left[\frac{K_0}{K_t(\boldsymbol{\theta})}\right], \end{aligned} \quad (9)$$

where the average is first taken over distance $\Delta\boldsymbol{\theta} = \boldsymbol{\theta} - \boldsymbol{\theta}_t$ and then over the gradient indices k . The variance is

maximized for fidelity $K_t(\boldsymbol{\theta}) \approx 0.6K_0$. For a fixed fidelity $K_t(\boldsymbol{\theta})$, the variance decreases linearly with number of parameters M and is independent of qubit number N . With $\text{Tr}(\mathcal{F}(\boldsymbol{\theta})^2) \geq \frac{\text{Tr}(\mathcal{F}(\boldsymbol{\theta}))^2}{M}$, we give the lower bound of the variance

$$\text{var}(\partial_k K_t(\boldsymbol{\theta})) \geq \frac{\text{Tr}(\mathcal{F}(\boldsymbol{\theta}))}{M^2} K_t(\boldsymbol{\theta})^2 \log \left[\frac{K_0}{K_t(\boldsymbol{\theta})} \right]. \quad (10)$$

We find a good match between Eq. (9) and simulated results in Fig. 2b for different types of PQCs, which improves with more qubits. It starts deviating from the analytic result when the variance of the gradient becomes close to the one given by a state sampled from a deep PQC with $\text{var}(\nabla K_t(\boldsymbol{\theta}_{\text{rand}})) = \frac{1}{2^{2N+1}}$ [7] (see Supplemental materials).

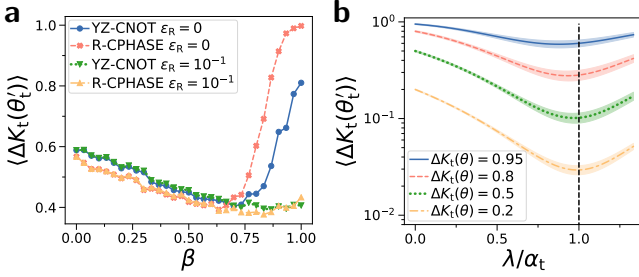


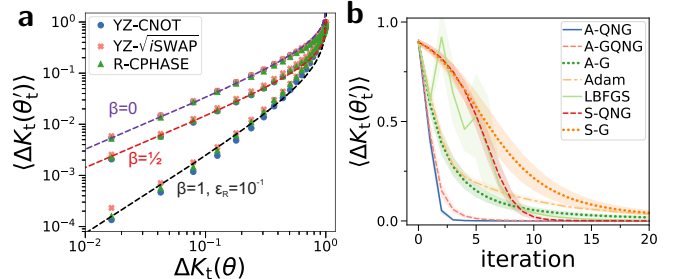
FIG. 3. **a)** Average infidelity $\langle \Delta K_t(\boldsymbol{\theta}_t') \rangle$ after one step of gradient ascent with adaptive learning rate (Eq. (8)) plotted against exponent β of the GQNG (Eq. (5)) for different types of PQCs and regularization parameter ϵ_R . Initial infidelity is $\Delta K_t(\boldsymbol{\theta}) = 0.9$. **b)** $\langle \Delta K_t(\boldsymbol{\theta}_t') \rangle$ (Eq. (1)) plotted against learning rate λ . We use gradient ascent update $\boldsymbol{\theta}_t' = \boldsymbol{\theta} + \lambda G_{\frac{1}{2}}(\boldsymbol{\theta})$ with GQNG. λ is normalized in respect to adaptive learning rate α_t (Eq. (8)), shown as vertical dashed line. Curves show various initial infidelities $\Delta K_t(\boldsymbol{\theta})$, with the shaded area being the standard deviation of $\Delta K_t(\boldsymbol{\theta}_t')$. Infidelity is averaged over 50 random instances of $\boldsymbol{\theta}_t$ for the YZ-CNOT PQC.

Results— We now demonstrate the performance of our VQA using numerical simulations [36, 37] with various types of expressive PQCs [24, 38]. In Fig. 3a, we plot the average infidelity after a single step of gradient ascent $\langle \Delta K_t(\boldsymbol{\theta}_t') \rangle$ (Eq. (1)) against β of the GQNG (Eq. (5)). Initially, the infidelity decreases with increasing β as more information from the QFIM is used. Without regularization $\epsilon_R = 0$, we observe a sharp increase of infidelity for $\beta > 0.6$ due to the ill-conditioned inverse of the QFIM. For larger β , this is mitigated by a non-zero regularization parameter $\epsilon_R = 10^{-1}$. Note that the regularization leads to a small increase in infidelity for $\beta \leq \frac{1}{2}$.

In Fig. 3b, we show the average infidelity after a single step of gradient ascent with the GQNG as function of learning rate λ for different initial infidelities $\Delta K_t(\boldsymbol{\theta})$. We find that α_t as calculated by Eq. (8) gives nearly the best learning rate even for larger infidelities. We find the same result when using the regular gradient or the QNG, as well as for target states that cannot be perfectly represented by the PQC (see Supplemental materials).

In Fig. 4a, we show $\langle \Delta K_t(\boldsymbol{\theta}_t') \rangle$ after one step of adaptive gradient ascent against initial infidelity $\Delta K_t(\boldsymbol{\theta})$ with the standard gradient ($\beta = 0$), the GQNG ($\beta = \frac{1}{2}$) and the QNG ($\beta = 1$ with regularization $\epsilon_R = 10^{-1}$). We find that different PQCs have nearly the same fidelity and the QNG outperforms GQNG and standard gradient at smaller initial infidelities. We numerically find that the data is fitted with $\Delta K_t(\boldsymbol{\theta}_t') = c[\frac{1}{4}\Delta\boldsymbol{\theta}^T \mathcal{F}(\boldsymbol{\theta}) \Delta\boldsymbol{\theta}]^\nu = -c \log^\nu [1 - \Delta K_t(\boldsymbol{\theta})]$, with $\nu = 1$ for $\beta = 0$, $\beta = \frac{1}{2}$ and $\nu = 1.5$ for the QNG with $\beta = 1$.

In Fig. 4b, we plot $\langle \Delta K_t(\boldsymbol{\theta}_t') \rangle$ against number of iterations of gradient ascent. We compare our adaptive training method with other established methods. Adaptive learning rates with QNG (A-QNG with $\beta = 1$ and regularization $\epsilon_R = 10^{-1}$) or GQNG (A-GQNG with $\beta = \frac{1}{2}$) outperforms other investigated methods and provides more than one order of magnitude smaller infidelities. It consistently performs well for different random instances, demonstrating a very low standard deviation in fidelity. We note that gradient ascent with adaptive learning rate and standard gradient (A-G with $\beta = 0$) still performs well, comparable to Adam and LBFGS. See Supplemental materials for further training data with other PQCs, different initial infidelities and logarithmic plots.



Discussion— We showed how to optimally train a PQC to represent a target quantum state. We found that the fidelity of quantum states can form Gaussian kernels. With this relation we derive adaptive learning rates that give the optimal magnitude of the gradient ascent update. The QNG provides the best direction for the gradient ascent step. We apply these methods to train different expressive PQCs that are able to represent a wide range of quantum states and are commonly used for VQAs [24, 38]. Combining adaptive learning rates and the QNG, we yield a lower number of iterations with an order of magnitude improvement in accuracy compared to other methods. This approach can be directly applied to a large range of VQAs, which have a subroutine that requires learning quantum states using the fidelity [25–29, 31, 39]. Future work can extend our methods to other cost functions such as Hamiltonians or the Hilbert-Schmidt test [40]. Adaptive learning rates and QNG combined could provide speed ups in training the variational quantum eigensolver for finding the ground states of Hamiltonians and molecules [3]. The QFIM \mathcal{F} needed for our method can be efficiently approximated using quantum computers [21, 23, 41, 42] as well as efficiently calculated classically [43].

The QNG uses the inverse of the QFIM, which can be ill-conditioned. To stabilize the QNG, it has to be regularized by adding the identity matrix with a small hyperparameter to the QFIM before inversion [21–23]. We show when regularization is necessary with the GQNG (Eq. (5)). For $\beta = \frac{1}{2}$, the GQNG $G_{\frac{1}{2}}(\boldsymbol{\theta}) = \mathcal{F}^{-\frac{1}{2}} \nabla K_t(\boldsymbol{\theta})$ does not require regularization while using quantum geometric information as much as possible. For $\beta \leq \frac{1}{2}$, the instability due to the inverse of the QFIM is canceled out by the quantum geometry of the PQC. Only for $\beta > \frac{1}{2}$ such as the QNG with $\beta = 1$, regularization has to be applied to take care of the ill-conditioned QFIM. While the QNG performs better for small infidelities, it performs comparable to the GQNG for larger infidelities. As the GQNG is inherently stable for $\beta = \frac{1}{2}$, the GQNG may be a good choice for initial training steps or for noisy systems.

While we discussed training in the context of PQC and VQAs, we note that our method is general and can also be applied for the control of quantum systems [44, 45]. Here, the task is to find the optimal driving protocol to generate a particular quantum state. By partitioning the driving protocol into discrete timesteps, the unitary that parameterizes the driving protocol has the form of a PQC, with the parameters being the amplitude of the driving protocol. Numerical optimization methods such as GRAPE [46] use gradients to find the best possible driving protocol. By using adaptive learning rates and QNG one could enhance those methods to find better protocols in a faster way.

A common feature of the cost function in many PQCs is that they form a narrow gorge, i.e. the cost function

deviates from its mean only in an exponentially small parameter space [8, 47]. These narrow gorges directly imply the existence of barren plateaus, i.e. the variance of the gradient vanishes exponentially with number of qubits, making training difficult for large quantum computers [7, 47]. Optimizing the PQC to represent a random state $|\psi_{\text{rand}}\rangle \in \mathcal{SU}(2^N)$ suffers from barren plateaus, which appear independently of the depth of the PQC [8]. The Gaussian kernel gives us now a functional description of the narrow gorge and allows us to calculate the variance of the gradients. We can ensure trainability and avoid the barren plateau problem by demanding that the state to be learned $|\psi_t\rangle$ is not random, but has a lower bounded fidelity with the initial state $K_t(\boldsymbol{\theta}) > \gamma$, where γ is the lower bound. We further assume that we are not too close to the optimal solution with $K_t(\boldsymbol{\theta}) < 0.6K_0$ where K_0 is the maximal possible fidelity. Then, Eq. (10) tells us that the variance of the gradient is lower bounded by

$$\text{var}(\nabla K_t(\boldsymbol{\theta})) \geq \frac{\text{Tr}(\mathcal{F})}{M^2} \log\left(\frac{K_0}{\gamma}\right) \gamma^2. \quad (11)$$

In particular, the lower bound of the variance is independent of the number of qubits N of the quantum computer and therefore the gradient does not vanish even when we scale up N . For training VQAs, a large enough γ is essential to ensure sufficiently large gradients. Here, we calculate γ explicitly for a type of VQA, the projected variational quantum dynamics method [25, 26]. This algorithm simulates the evolution of the state $|\psi(\boldsymbol{\theta})\rangle$ with a Hamiltonian H (see Supplemental materials for training examples). It evolves the PQC using a single Trotter step with time Δt and then variationally learns to represent the evolved state $|\psi_t\rangle = \exp(-iH\Delta t)|\psi(\boldsymbol{\theta})\rangle$ via the fidelity as cost function. This process is then repeated N_T times to evolve for a total time $T = N_T\Delta t$. Here, we find that the initial fidelity is lower bounded by

$$\gamma = 1 - \frac{1}{4}(\Delta E \Delta t)^2, \quad (12)$$

where ΔE is the energy difference between the largest and smallest eigenenergies of H whose eigenstates have non-zero overlap with $|\psi(\boldsymbol{\theta})\rangle$ (see Supplemental materials). By choosing a small enough Δt and ΔE , one can ensure sufficiently large gradients and that the VQA is free of barren plateaus. This opens up the possibility to train these VQAs on large-scale quantum computers. An interesting application would be to simulate the dynamics of complicated many-body systems that are beyond the reach of current classical simulation methods. To reach this goal, future work has to engineer PQCs that can represent the time evolved states for a large number of qubits. Adaptively chosen PQCs [48] or PQCs tailored to the specific problem could enhance the representation power. Hybrid states as linear combination

of quantum states generated using the problem Hamiltonian could systematically create an ansatz suited for the problem [13–15]. We note that training VQAs without a lower bounded fidelity is expected to be difficult, as most likely training will be stuck in the barren plateau. In this case, other types of cost function may provide a way out of the barren plateau [8].

As a tangential observation, we note that Eq. (9) enables us to calculate $\text{Tr}(\mathcal{F}^2)$ by measuring the variance of the gradients.

Finally, our results have direct implications for quantum machine learning, which utilizes quantum features to enhance machine learning. Here, data is embedded as parameters of the PQC and the fidelity of the quantum states is used as a nonlinear feature map [49–51]. The Gaussian (or radial basis function) kernel we provide is such a nonlinear feature map, which has important applications in various classical machine learning models such as support vector machines [52]. In a quantum setting, these kernels have been so far only proposed with coherent states [53–55]. As advantage compared to coherent states, PQCs can adjust the QFIM and the weight matrix of the Gaussian kernel by changing the structure of the PQC [24]. Given that these kernels can be efficiently computed classically, they are unlikely to provide a direct quantum advantage from data in machine learning [50, 54, 56]. However, with increasing distance in parameter space the approximation as Gaussian is less accurate and the kernel may acquire the features needed to provide quantum advantage [56]. The kernel could be immediately realized with current quantum hardware for tasks in quantum machine learning [50, 51, 57, 58] and Gaussian processes [55, 59] to provide novel applications of quantum computers.

Python code for the numerical calculations are available on Github [60].

We acknowledge discussions with Giuseppe Carleo, Kiran Khosla, Christopher Self and Alistair Smith. This work is supported by a Samsung GRC project and the UK Hub in Quantum Computing and Simulation, part of the UK National Quantum Technologies Programme with funding from UKRI EPSRC grant EP/T001062/1.

A variational eigenvalue solver on a photonic quantum processor, *Nature communications* **5**, 4213 (2014).

- [4] A. Kandala, A. Mezzacapo, K. Temme, M. Takita, M. Brink, J. M. Chow, and J. M. Gambetta, Hardware-efficient variational quantum eigensolver for small molecules and quantum magnets, *Nature* **549**, 242 (2017).
- [5] J. R. McClean, J. Romero, R. Babbush, and A. Aspuru-Guzik, The theory of variational hybrid quantum-classical algorithms, *New Journal of Physics* **18**, 023023 (2016).
- [6] M. Cerezo, A. Arrasmith, R. Babbush, S. C. Benjamin, S. Endo, K. Fujii, J. R. McClean, K. Mitarai, X. Yuan, L. Cincio, *et al.*, Variational quantum algorithms, *arXiv preprint arXiv:2012.09265* (2020).
- [7] J. R. McClean, S. Boixo, V. N. Smelyanskiy, R. Babbush, and H. Neven, Barren plateaus in quantum neural network training landscapes, *Nature communications* **9**, 4812 (2018).
- [8] M. Cerezo, A. Sone, T. Volkoff, L. Cincio, and P. J. Coles, Cost function dependent barren plateaus in shallow parametrized quantum circuits, *Nature Communications* **12**, 1 (2021).
- [9] C. O. Marrero, M. Kieferová, and N. Wiebe, Entanglement induced barren plateaus, *arXiv:2010.15968* (2020).
- [10] S. Wang, E. Fontana, M. Cerezo, K. Sharma, A. Sone, L. Cincio, and P. J. Coles, Noise-induced barren plateaus in variational quantum algorithms, *arXiv:2007.14384* (2020).
- [11] L. Bittel and M. Kliesch, Training variational quantum algorithms is np-hard – even for logarithmically many qubits and free fermionic systems, *arXiv:2101.07267* (2021).
- [12] K. Bharti, Quantum assisted eigensolver, *arXiv:2009.11001* (2020).
- [13] K. Bharti and T. Haug, Quantum assisted simulator, *arXiv:2011.06911* (2020).
- [14] K. Bharti and T. Haug, Iterative quantum assisted eigensolver, *arXiv:2010.05638* (2020).
- [15] T. Haug and K. Bharti, Generalized quantum assisted simulator, *arXiv:2011.14737* (2020).
- [16] J. W. Z. Lau, T. Haug, L. C. Kwek, and K. Bharti, Nisq algorithm for hamiltonian simulation via truncated taylor series, *arXiv:2103.05500* (2021).
- [17] K. H. Lim, T. Haug, L. C. Kwek, and K. Bharti, Fast-forwarding with nisq processors without feedback loop, *arXiv:2104.01931* (2021).
- [18] J. Stokes, J. Izaac, N. Killoran, and G. Carleo, Quantum natural gradient, *Quantum* **4**, 269 (2020).
- [19] B. Koczor and S. C. Benjamin, Quantum natural gradient generalised to non-unitary circuits, *arXiv preprint arXiv:1912.08660* (2019).
- [20] N. Yamamoto, On the natural gradient for variational quantum eigensolver, *arXiv:1909.05074* (2019).
- [21] B. van Straaten and B. Koczor, Measurement cost of metric-aware variational quantum algorithms, *arXiv:2005.05172* (2020).
- [22] D. Wierichs, C. Gogolin, and M. Kastoryano, Avoiding local minima in variational quantum eigensolvers with the natural gradient optimizer, *arXiv:2004.14666* (2020).
- [23] J. Gacon, C. Zoufal, G. Carleo, and S. Woerner, Simultaneous perturbation stochastic approximation of the quantum fisher information, *arXiv:2103.09232* (2021).
- [24] T. Haug, K. Bharti, and M. Kim, Capacity and

* thaug@ic.ac.uk

- [1] J. Preskill, Quantum computing in the nisq era and beyond, *Quantum* **2**, 79 (2018).
- [2] K. Bharti, A. Cervera-Lierta, T. H. Kyaw, T. Haug, S. Alperin-Lea, A. Anand, M. Degroote, H. Heimonen, J. S. Kottmann, T. Menke, W.-K. Mok, S. Sim, L.-C. Kwek, and A. Aspuru-Guzik, Noisy intermediate-scale quantum (nisq) algorithms, *arXiv:2101.08448* (2021).
- [3] A. Peruzzo, J. McClean, P. Shadbolt, M.-H. Yung, X.-Q. Zhou, P. J. Love, A. Aspuru-Guzik, and J. L. Obrien,

quantum geometry of parametrized quantum circuits, arXiv:2102.01659 (2021).

[25] M. Otten, C. L. Cortes, and S. K. Gray, Noise-resilient quantum dynamics using symmetry-preserving ansatzes, arXiv preprint arXiv:1910.06284 (2019).

[26] S. Barison, F. Vicentini, and G. Carleo, An efficient quantum algorithm for the time evolution of parameterized circuits, arXiv:2101.04579 (2021).

[27] J. Gibbs, K. Gili, Z. Holmes, B. Commeau, A. Arrasmith, L. Cincio, P. J. Coles, and A. Sornborger, Long-time simulations with high fidelity on quantum hardware, arXiv:2102.04313 (2021).

[28] Z. Holmes, A. Arrasmith, B. Yan, P. J. Coles, A. Albrecht, and A. T. Sornborger, Barren plateaus preclude learning scramblers, arXiv:2009.14808 (2020).

[29] M. Benedetti, D. Garcia-Pintos, O. Perdomo, V. Leyton-Ortega, Y. Nam, and A. Perdomo-Ortiz, A generative modeling approach for benchmarking and training shallow quantum circuits, *npj Quantum Information* **5**, 1 (2019).

[30] H.-L. Huang, Y. Du, M. Gong, Y. Zhao, Y. Wu, C. Wang, S. Li, F. Liang, J. Lin, Y. Xu, *et al.*, Experimental quantum generative adversarial networks for image generation, arXiv:2010.06201 (2020).

[31] J. Romero, J. P. Olson, and A. Aspuru-Guzik, Quantum autoencoders for efficient compression of quantum data, *Quantum Sci. Technol.* **2**, 045001 (2017).

[32] O. Higgott, D. Wang, and S. Brierley, Variational quantum computation of excited states, *Quantum* **3**, 156 (2019).

[33] J. J. Meyer, Fisher information in noisy intermediate-scale quantum applications, 2103.15191 (2021).

[34] J. Liu, H. Yuan, X.-M. Lu, and X. Wang, Quantum fisher information matrix and multiparameter estimation, *Journal of Physics A: Mathematical and Theoretical* **53**, 023001 (2019).

[35] W. G. Brown and L. Viola, Convergence rates for arbitrary statistical moments of random quantum circuits, *Physical review letters* **104**, 250501 (2010).

[36] X.-Z. Luo, J.-G. Liu, P. Zhang, and L. Wang, Yao. jl: Extensible, efficient framework for quantum algorithm design, *Quantum* **4**, 341 (2020).

[37] J. R. Johansson, P. D. Nation, and F. Nori, Qutip: An open-source python framework for the dynamics of open quantum systems, *Computer Physics Communications* **183**, 1760 (2012).

[38] S. Sim, P. D. Johnson, and A. Aspuru-Guzik, Expressibility and entangling capability of parameterized quantum circuits for hybrid quantum-classical algorithms, *Advanced Quantum Technologies* **2**, 1900070 (2019).

[39] T. Jones, S. Endo, S. McArdle, X. Yuan, and S. C. Benjamin, Variational quantum algorithms for discovering hamiltonian spectra, *Physical Review A* **99**, 062304 (2019).

[40] S. Khatri, R. LaRose, A. Poremba, L. Cincio, A. T. Sornborger, and P. J. Coles, Quantum-assisted quantum compiling, *Quantum* **3**, 140 (2019).

[41] M. Cerezo, A. Sone, J. L. Beckey, and P. J. Coles, Sub-quantum fisher information, arXiv preprint arXiv:2101.10144 (2021).

[42] J. L. Beckey, M. Cerezo, A. Sone, and P. J. Coles, Variational quantum algorithm for estimating the quantum fisher information, arXiv:2010.10488 (2020).

[43] T. Jones, Efficient classical calculation of the quantum natural gradient, arXiv preprint arXiv:2011.02991 (2020).

[44] S. J. Glaser, U. Boscain, T. Calarco, C. P. Koch, W. Köckenberger, R. Kosloff, I. Kuprov, B. Luy, S. Schirmer, T. Schulte-Herbrüggen, *et al.*, Training schrödinger's cat: quantum optimal control, *The European Physical Journal D* **69**, 1 (2015).

[45] V. Bastidas, T. Haug, C. Gravel, L.-C. Kwek, W. Munro, and K. Nemoto, Fully-programmable universal quantum simulator with a one-dimensional quantum processor, arXiv:2009.00823 (2020).

[46] S. Machnes, U. Sander, S. J. Glaser, P. De Fouquieres, A. Gruslys, S. Schirmer, and T. Schulte-Herbrüggen, Comparing, optimizing, and benchmarking quantum-control algorithms in a unifying programming framework, *Physical Review A* **84**, 022305 (2011).

[47] A. Arrasmith, Z. Holmes, M. Cerezo, and P. J. Coles, Equivalence of quantum barren plateaus to cost concentration and narrow gorges, arXiv:2104.05868 (2021).

[48] H. R. Grimsley, S. E. Economou, E. Barnes, and N. J. Mayhall, An adaptive variational algorithm for exact molecular simulations on a quantum computer, *Nature communications* **10**, 1 (2019).

[49] J. Biamonte, P. Wittek, N. Pancotti, P. Rebentrost, N. Wiebe, and S. Lloyd, Quantum machine learning, *Nature* **549**, 195 (2017).

[50] M. Schuld and N. Killoran, Quantum machine learning in feature hilbert spaces, *Physical review letters* **122**, 040504 (2019).

[51] M. Schuld, R. Sweke, and J. J. Meyer, Effect of data encoding on the expressive power of variational quantum-machine-learning models, *Physical Review A* **103**, 032430 (2021).

[52] I. Goodfellow, Y. Bengio, A. Courville, and Y. Bengio, *Deep learning*, Vol. 1 (MIT press Cambridge, 2016).

[53] R. Chatterjee and T. Yu, Generalized coherent states, reproducing kernels, and quantum support vector machines, arXiv:1612.03713 (2016).

[54] M. Schuld, Quantum machine learning models are kernel methods, arXiv:2101.11020 (2021).

[55] M. Otten, I. R. Goumire, B. W. Priest, G. F. Chapline, and M. D. Schneider, Quantum machine learning using gaussian processes with performant quantum kernels, arXiv preprint arXiv:2004.11280 (2020).

[56] H.-Y. Huang, M. Broughton, M. Mohseni, R. Babbush, S. Boixo, H. Neven, and J. R. McClean, Power of data in quantum machine learning, arXiv:2011.01938 (2020).

[57] V. Havlíček, A. D. Córcoles, K. Temme, A. W. Harrow, A. Kandala, J. M. Chow, and J. M. Gambetta, Supervised learning with quantum-enhanced feature spaces, *Nature* **567**, 209 (2019).

[58] C. Blank, D. K. Park, J.-K. K. Rhee, and F. Petruccione, Quantum classifier with tailored quantum kernel, *npj Quantum Information* **6**, 1 (2020).

[59] C. E. Rasmussen and C. K. I. Williams, *Gaussian Processes for Machine Learning (Adaptive Computation and Machine Learning)* (The MIT Press, 2005).

[60] T. Haug, Optimal quantum learning, <https://github.com/txhaug/optimal-quantum-learning>.

Parameterized quantum circuits

The PQCs used in the main text are described in Fig.5. The PQCs are given by $\psi(\boldsymbol{\theta}) = U(\boldsymbol{\theta})|0\rangle^{\otimes N} = \prod_{l=p}^1 [W_l V_l(\theta_l)]|0\rangle^{\otimes N}$, which consist of p layers of entangling gates W_l and parameterized rotations $V_l(\theta_l)$. The parameters $\boldsymbol{\theta}$ are chosen randomly.

Further data on variance of gradient

In Fig.6a, we show the variance of the gradient as function of parameter norm $\boldsymbol{\theta}^T \mathcal{F} \boldsymbol{\theta}$. We see a good match with the analytic formula. For large $\boldsymbol{\theta}^T \mathcal{F} \boldsymbol{\theta}$, we see deviation from the analytic result, as the variance of the gradient approaches the value given by a random state sampled from a sufficiently deep PQC with $\text{var}(\nabla K_t(\boldsymbol{\theta}_{\text{rand}})) = \frac{1}{2^{2N+1}}$ [7].

Further data on adaptive learning rate

In this section we show further numerical simulations. We compare the adaptive gradient ascent using the GQNG, regular gradient and QNG in Fig.7. We find for all types of gradients, the adaptive gradient ascent finds the nearly optimal learning rate.

Now, we choose a target state that cannot be perfectly represented by the PQC, i.e. $K_0 = \max_{\boldsymbol{\theta}} K_t(\boldsymbol{\theta}) < 1$. In Fig.8, we investigate the learning rate λ normalized to the optimal one α_t for $K_0 = 0.5$. We find for both types of gradients, the adaptive gradient ascent finds the nearly optimal learning rate.

Further training data

In this section we show further data for the training of the VQA. We show training of our VQA in Fig.9 for both linear and logarithmic plots for the YZ-CNOT PQC. We see that QNG and GQNG with adaptive learning rates provides about one order of magnitude smaller infidelities compared to other methods.

We show further training of our VQA in Fig.10 for the R-CPHASE PQC. We find similar trajectories as before, however in general the infidelities are a bit higher. This may be related to the fact that the R-CPHASE PQC has a QFIM with more smaller eigenvalues compared to the YZ-CNOT PQC. This may affect training adversely here.

In Fig.11, we compare QNG (A-QNG), GQNG (A-GQNG) and standard gradient (A-G) with adaptive learning rate against Adam and LBFGS for different values of initial infidelity. We find superior performance of A-QNG and A-GQNG for higher infidelities as well. A-G performs comparable to Adam.

In Fig.12, we compare training with A-QNG and A-GQNG for different initial infidelities $\Delta K_t(\boldsymbol{\theta})$. We can train the PQC even for very high infidelities. Note that the Gaussian kernel approximation breaks down for $\Delta K_t(\boldsymbol{\theta}) > 1 - \frac{1}{2^N} \approx 0.999$. However, training is still possible then, although at a slower rate.

Now, again the target state to be learned cannot be perfectly represented by PQC, i.e. $K_0 = \max_{\boldsymbol{\theta}} K_t(\boldsymbol{\theta}) \approx 0.5$. We show the trajectories for the YZ-CNOT PQC in Fig.13. We note that A-QNG and A-GQNG find the solution faster compared to other algorithms.

PQC with Gaussian kernel

We show a PQC with Gaussian kernel that can be analytically calculated with the following N qubit quantum state

$$|\psi(\boldsymbol{\theta})\rangle = \bigotimes_{n=1}^N \left(\cos\left(\frac{\theta_n}{2}\right) |0\rangle + \sin\left(\frac{\theta_n}{2}\right) |1\rangle \right). \quad (13)$$

The fidelity of two states parameterized by $\boldsymbol{\theta}, \boldsymbol{\theta}'$ is given by

$$K(\boldsymbol{\theta}, \boldsymbol{\theta}') = |\langle \psi(\boldsymbol{\theta}) | \psi(\boldsymbol{\theta}') \rangle|^2 = \prod_{n=1}^N \left(1 + \frac{1}{2} \cos(\Delta\theta_n) \right) \quad (14)$$

where we define $\Delta\boldsymbol{\theta} = \boldsymbol{\theta} - \boldsymbol{\theta}'$ as the difference between the two parameter sets. We now assume $|\Delta\theta_n| \ll 1$ and that all the differences of the parameters are equal $\Delta\theta_1 = \dots = \Delta\theta_N$. We then find in the limit of many qubits N

$$K(\boldsymbol{\theta}, \boldsymbol{\theta}') \approx \prod_{n=1}^N \left(1 - \frac{1}{4} \Delta\theta_n^2 \right) \xrightarrow{N \rightarrow \infty} \exp\left(-\frac{1}{4} \Delta\boldsymbol{\theta}^T \Delta\boldsymbol{\theta}\right). \quad (15)$$

The QFIM of above model is $\mathcal{F}(\boldsymbol{\theta}) = I$, I being the identity matrix. We can now modify the model to describe a generic PQC with the QFIM \mathcal{F} . We now assume that the parameters of the PQC $\boldsymbol{\theta}$ are not independent, but are related via $\boldsymbol{\theta} = \mathcal{F}^{\frac{1}{2}} \boldsymbol{\mu}$, where $\boldsymbol{\mu}$ is some N dimensional parameter. We find for the transformed parameters $\boldsymbol{\mu}$

$$K(\boldsymbol{\mu}, \boldsymbol{\mu}') \approx \exp\left(-\frac{1}{4} \Delta\boldsymbol{\mu}^T \mathcal{F} \Delta\boldsymbol{\mu}\right), \quad (16)$$

where $\Delta\boldsymbol{\mu} = \boldsymbol{\mu} - \boldsymbol{\mu}'$ and we used $|\mathcal{F}^{\frac{1}{2}} \boldsymbol{\mu}|^2 = \boldsymbol{\mu}^T \mathcal{F} \boldsymbol{\mu}$. A first order Taylor expansion gives us

$$K(\boldsymbol{\mu}, \boldsymbol{\mu}') \approx \exp\left(-\frac{1}{4} \Delta\boldsymbol{\mu}^T \mathcal{F} \Delta\boldsymbol{\mu}\right) \approx 1 - \frac{1}{4} \Delta\boldsymbol{\mu}^T \mathcal{F} \Delta\boldsymbol{\mu}, \quad (17)$$

which is the relation between fidelity and parameter distance for the QFIM [33, 34].

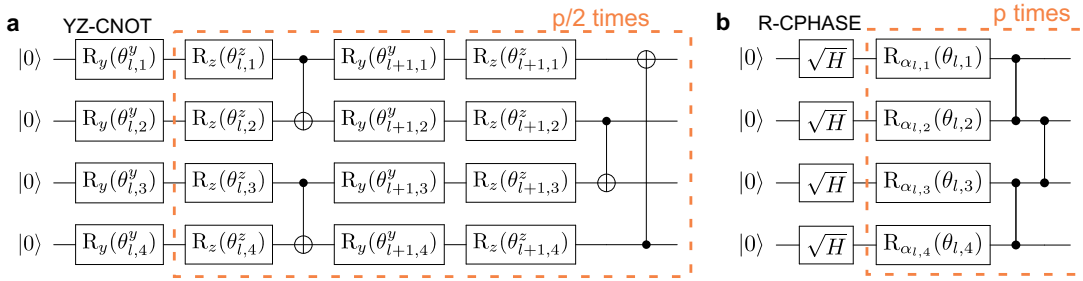


FIG. 5. Description of PQCs used in the main text. **a)** YZ-CNOT consists of p layers, with each layer having Y and Z rotations applied on each qubit, and CNOT gates between neighboring qubits applied in an alternating fashion. For odd layer number l , CNOT gate is applied between qubit $2n-1$ and $2n$, for even l CNOT is applied on $2n$ and $2n+1$. For YZ- \sqrt{i} SWAP, the CNOT gates are replaced with \sqrt{i} SWAP gates. **b)** R-CPHASE PQC, which consists of an initial layer of $\pi/2$ rotation around the y -axis, followed by p layers. Each layer consists of randomly chosen rotations with σ^x , σ^y or σ^z , followed by CPHASE gates applied as a chain of nearest-neighbors.

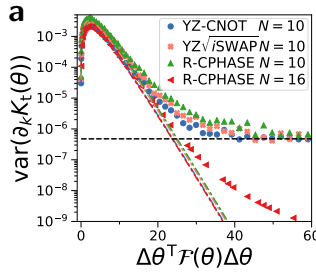


FIG. 6. **a)** Variance of gradient $\text{var}(\partial_k K_t(\theta))$ against parameter norm $\Delta\theta^T \mathcal{F}(\theta) \Delta\theta$ for different types of PQCs. Dashed line is the analytic formula Eq. (41) for the variance. The dashed horizontal line is the variance of the gradient for states of a random PQC $\text{var}(\nabla K_t(\theta_{\text{rand}})) = \frac{1}{2^{2N+1}}$ [7]. Number of layers $p = 20$ for R-CPHASE $N = 10$, $p = 16$ for $N = 16$, else $p = 10$. Average over 50 random instances of θ_t .

Generalized quantum natural gradient

The generalized quantum natural gradient (GQNG) is given by

$$G_\beta(\theta) = \mathcal{F}^{-\beta}(\theta) \nabla K_t(\theta), \quad (18)$$

with $\beta \in [0, 1]$, the derivative of the fidelity $\nabla K_t(\theta)$ and the QFIM $\mathcal{F}(\theta)$. Standard gradient ascent is $G_0(\theta) = \nabla K_t(\theta)$, whereas the QNG is $G_1(\theta) = \mathcal{F}^{-1}(\theta) \nabla K_t(\theta)$ [18, 20]. The standard gradient is reliable, however it can require many update steps before convergence. The QNG gives the optimal gradient in parameter space, however it is unstable without regularization. We trace this instability back to the inverse of the QFIM $\mathcal{F}^{-1}(\theta)$, which when ill conditioned is highly sensitive to small changes in parameter θ . A common approach is to take care of the ill-conditioned QFIM is by adding the identity matrix to the QFIM before inversion $\mathcal{F}' = \mathcal{F} + \epsilon_R I$, where I is the identity matrix and ϵ_R a small hyperparameter. By choosing appropriate $\epsilon_R > 0$ the QNG can become stable. We now want to investigate

when regularization is necessary as a function of β in the first place. β allows us to tune the trade-off between stability and optimal updates. With the Gaussian kernel, a gradient ascent update $\theta' = \theta + \alpha G_\beta(\theta)$ gives us the fidelity

$$K_t(\theta') = K_0 \exp\left[-\frac{1}{4}(\Delta\theta + \alpha G_\beta(\theta))^T \mathcal{F}(\theta) (\Delta\theta + \alpha G_\beta(\theta))\right], \quad (19)$$

where K_0 is the maximal possible fidelity and $\Delta\theta = \theta - \theta_t$. For convenience, in the following we do not explicitly write the θ parameter for $\mathcal{F}(\theta)$ and $\nabla K_t(\theta)$ and we set $\epsilon_R = 0$

$$\begin{aligned} K_t(\theta') &= K_t(\theta) \exp\left[-\frac{\alpha}{4}(\alpha G_\beta^T \mathcal{F} G_\beta + G_\beta^T \mathcal{F} \Delta\theta + \Delta\theta^T \mathcal{F} G_\beta)\right] \\ &= K_t(\theta) \exp\left[-\frac{\alpha}{4}(\alpha \nabla K_t^T \mathcal{F}^{1-2\beta} \nabla K_t + 2\Delta\theta^T \mathcal{F}^{1-\beta} \nabla K_t)\right], \end{aligned}$$

where we used $\mathcal{F}^T = \mathcal{F}$. For choice $\beta \leq \frac{1}{2}$, the updated fidelity does not contain any terms with $\mathcal{F}^{-\delta}$ having a negative exponent, which could cause instabilities. Thus, gradient ascent with $\beta = \frac{1}{2}$ and $G_{\frac{1}{2}}(\theta) = \mathcal{F}^{-\frac{1}{2}} \nabla K_t(\theta)$ is stable without the need of regularization. For $\beta > \frac{1}{2}$, $\epsilon_R > 0$ has to be chosen to take care of the ill-conditioned inverse of the QFIM.

Gradient update rule

Here, we derive the adaptive learning rates for gradient ascent. We would like to solve the optimisation problem $\theta_t = \text{argmax}_\theta |\langle \psi(\theta) | \psi_t \rangle|^2$. First, we assume that $\max_\theta |\langle \psi(\theta) | \psi_t \rangle|^2 = K_0 = 1$, i.e. the PQC is able to perfectly represent the state. We relax $K_0 < 1$ further below. For the initial parameter θ we have a fidelity $K_t(\theta)$. Gradient ascent with the GQNG uses the update rule for the next parameter θ_1

$$\theta_1 = \theta + \alpha_1 G_\beta(\theta), \quad (20)$$

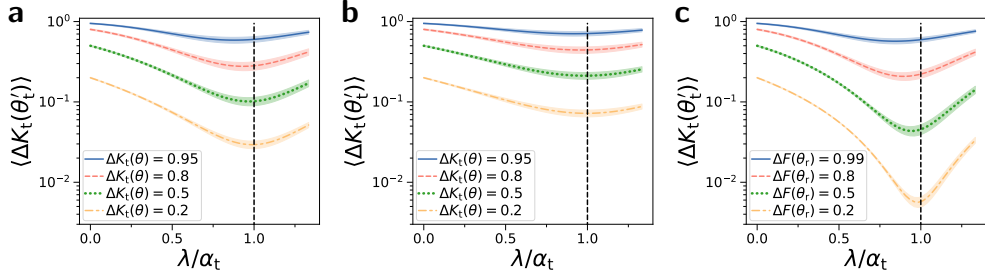


FIG. 7. Average infidelity after one step of gradient ascent step $\langle \Delta K_t(\theta'_t) \rangle$ plotted against learning rate λ , for gradient ascent update $\theta'_t = \theta + \lambda G_\beta(\theta)$. λ is normalized in respect to analytically calculated learning rate α_t (Eq. (35)), shown as vertical dashed line. Curves show various initial infidelities $\Delta K_t(\theta)$, with shaded area being the standard deviation of $\Delta K_t(\theta'_t)$. Infidelity averaged over 50 random instances of YZ-CNOT PQC. We show **a)** the GQNG $\beta = \frac{1}{2}$, **b)** the regular gradient $\beta = 0$ and **c)** QNG $\beta = 1$ with regularization $\epsilon_R = 10^{-1}$.

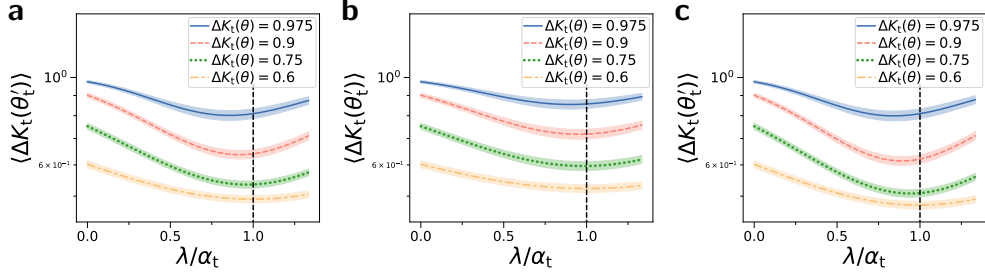


FIG. 8. Target state to be learned cannot be perfectly represented by PQC, i.e. $K_0 = \max_\theta K_t(\theta) \approx 0.5$. Average infidelity after one step of gradient ascent step $\langle \Delta K_t(\theta'_t) \rangle$ plotted against learning rate λ , for gradient ascent update $\theta'_t = \theta + \lambda G_\beta(\theta)$. λ is normalized in respect to analytically calculated learning rate α_t , shown as vertical dashed line. Curves show various initial infidelities $\Delta K_t(\theta)$, with shaded area being the standard deviation of $\Delta K_t(\theta'_t)$. Infidelity averaged over 50 random instances of YZ-CNOT PQC. We show **a)** the GQNG $\beta = \frac{1}{2}$, **b)** the regular gradient $\beta = 0$ and **c)** QNG $\beta = 1$ with regularization $\epsilon_R = 10^{-1}$.

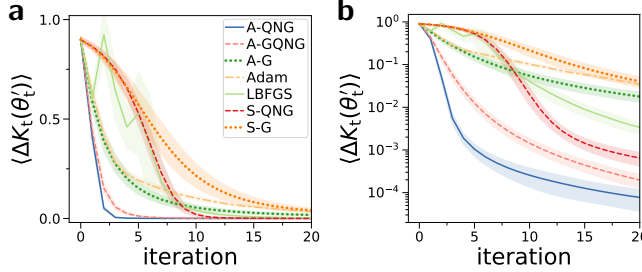


FIG. 9. Training with YZ-CNOT PQC. **a)** Linear Plot **b)** Logarithmic plot. Mean infidelity $\langle \Delta K_t(\theta'_t) \rangle$ against number of iterations of gradient ascent. Shaded area is the standard deviation over 50 instances of training. We compare different optimization methods against each other. We find that adaptive gradient ascent with QNG (A-QNG, $\beta = 1$, $\epsilon_R = 10^{-1}$) or GQNG (A-GQNG, $\beta = \frac{1}{2}$, $\epsilon_R = 0$) performs best by a large margin, followed by adaptive method with regular gradient (A-G). Standard optimization methods such as Adam and L-BFGS perform comparable to A-G. Initial infidelity is $\Delta K_t(\theta) = 0.9$, $N = 10$ and $p = 10$.

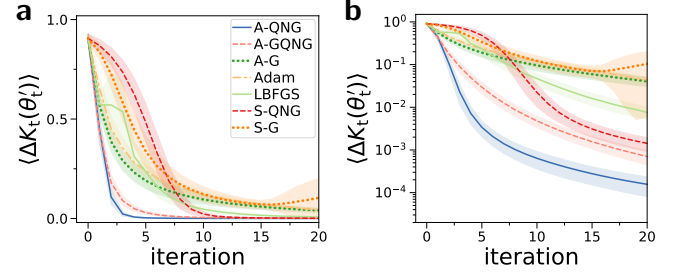


FIG. 10. Training with R-CPHASE PQC. **a)** Linear Plot **b)** Logarithmic plot. Mean infidelity $\langle \Delta K_t(\theta'_t) \rangle$ against number of iterations of gradient ascent. Initial infidelity is $\Delta K_t(\theta) = 0.9$, $N = 10$ and $p = 20$.

follows a Gaussian kernel, and we would like to choose α_1 such that this update is as close as possible to the correct solution $\theta_1 \approx \theta_t$. Given the Gaussian kernel, we have

$$K_t(\theta) = e^{-\frac{1}{4} \Delta \theta^T \mathcal{F}(\theta) \Delta \theta}. \quad (21)$$

with learning rate α_1 and GQNG $G_\beta(\theta) = \mathcal{F}^{-\beta}(\theta) \nabla K_t(\theta)$. We assume now that the fidelity

where we defined the distance between target parameter and initial parameter $\Delta \theta = \theta_t - \theta$. We then find by

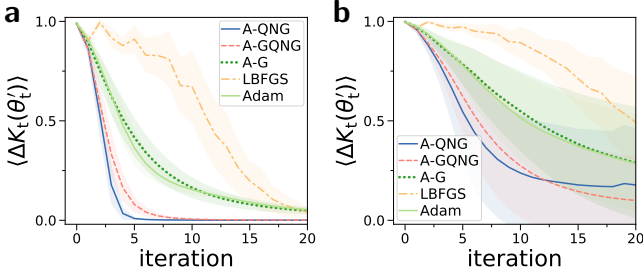


FIG. 11. Mean infidelity $\langle \Delta K_t(\theta'_t) \rangle$ against number of iterations of gradient ascent. Shaded area is the standard deviation over 50 instances of training. We compare QNG, GQNG and standard gradient with adaptive learning rate against Adam and LBFGS. **a)** Initial infidelity $\Delta K_t(\theta) = 0.99$ **b)** $\Delta K_t(\theta) = 0.999$. The PQC used is YZ-CNOT with $N = 10$ and $p = 10$. The regularization for A-QNG is $\epsilon_R = 10^{-1}$.

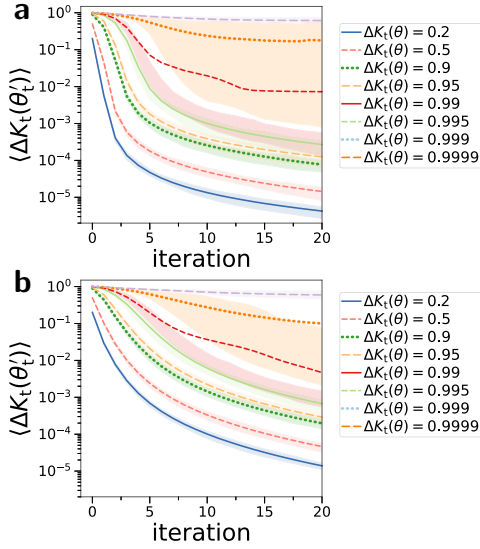


FIG. 12. Different initial infidelities $\Delta K_t(\theta)$ for **a)** A-QNG ($\epsilon_R = 10^{-1}$) and **b)** A-GQNG ($\beta = \frac{1}{2}$). Mean infidelity $\langle \Delta K_t(\theta'_t) \rangle$ against number of iterations of gradient ascent. Shaded area is the 20 and 80 percentile over 50 instances of training. The PQC is YZ-CNOT with $N = 10$ and $p = 10$.

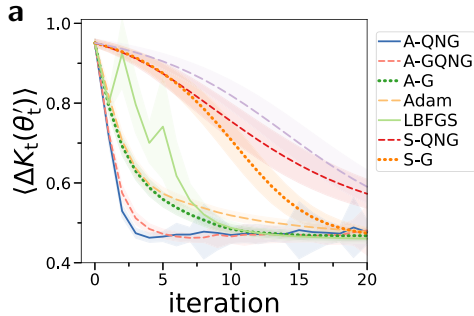


FIG. 13. Training with YZ-CNOT PQC where target state cannot be learned perfectly, i.e. $K_0 = \max_{\theta} K_t(\theta) \approx 0.5$. Mean infidelity $\langle \Delta K_t(\theta'_t) \rangle$ against number of iterations of gradient ascent for different optimization routines. Initial infidelity is $\Delta K_t(\theta) = 0.95$, $N = 10$ and $p = 10$.

applying the logarithm

$$-4 \log(K_t(\theta)) = \Delta \theta^T \mathcal{F}(\theta) \Delta \theta. \quad (22)$$

A reordering of Eq. (20) gives us

$$\Delta \theta = \alpha_1 G_\beta(\theta) \quad (23)$$

We now multiply both sides with $\mathcal{F}^{\frac{1}{2}}(\theta)$ and get

$$\mathcal{F}^{\frac{1}{2}}(\theta) \Delta \theta = \alpha_1 \mathcal{F}^{\frac{1}{2}}(\theta) G_\beta(\theta), \quad (24)$$

followed by taking square on both sides

$$\Delta \theta^T \mathcal{F}(\theta) \Delta \theta = \alpha_1^2 G_\beta(\theta)^T \mathcal{F}(\theta) \nabla G_\beta(\theta), \quad (25)$$

where we used $|\mathcal{F}^{\frac{1}{2}} \mu|^2 = \mu^T \mathcal{F} \mu$. We insert Eq. (22) and get

$$\alpha_1 = \frac{2 \sqrt{-\log(K_t(\theta))}}{\sqrt{G_\beta(\theta)^T \mathcal{F}(\theta) G_\beta(\theta)}}, \quad (26)$$

with the first update rule

$$\theta_1 = \theta + \alpha_1 G_\beta(\theta). \quad (27)$$

We assumed for above calculations that the PQC is able to represent the target quantum state perfectly, i.e. $\max_{\theta} |\langle \psi(\theta) | \psi_t \rangle|^2 = 1$. If this is not the case, we have to adjust the learning rate to take this into account.

Assume the target state is given by

$$|\psi_t\rangle = \sqrt{K_0} |\psi(\theta_t)\rangle + \sqrt{1 - K_0} |\psi_o\rangle, \quad (28)$$

where $|\psi_o\rangle$ is some state that is orthogonal to any other state that can be represented by the PQC, i.e. $|\langle \psi_o | \psi(\theta) \rangle|^2 = 0 \forall \theta$ and K_0 is the maximal possible fidelity of the PQC. Then, the first update rule is moving in the correct direction, however overshoots the target parameters. We now calculate the update rule that takes this into account. We find

$$K_t(\theta) = K_0 e^{-\frac{1}{4} \Delta \theta^T \mathcal{F}(\theta) \Delta \theta} \quad (29)$$

$$K_t(\theta_1) = K_0 e^{-\frac{1}{4} (\theta_1 - \theta_t)^T \mathcal{F}(\theta) (\theta_1 - \theta_t)} \quad (30)$$

where $K_t(\theta_1)$ is the fidelity after applying the first update rule. Now our goal is to find the corrected update rule

$$\theta_t = \theta + \alpha_t G_\beta(\theta), \quad (31)$$

with updated learning rate α_t . By subtracting the two update rules we get

$$\theta_1 - \theta_t = (\alpha_1 - \alpha_t) G_\beta(\theta). \quad (32)$$

We insert above equations into the fidelities and get

$$K_t(\theta) = K_0 e^{-\frac{1}{4} \alpha_t^2 G_\beta^T \mathcal{F} G_\beta} \quad (33)$$

$$K_t(\boldsymbol{\theta}_1) = K_0 e^{-\frac{1}{4}(\alpha_t - \alpha_t)^2 G_\beta^T \mathcal{F} G_\beta} \quad (34)$$

By dividing above equations, we can solve for α_t and find

$$\alpha_t = \frac{1}{2} \left(\frac{4}{\alpha_1 G_\beta(\boldsymbol{\theta})^T \mathcal{F}(\boldsymbol{\theta}) G_\beta(\boldsymbol{\theta})} \log \left(\frac{K_t(\boldsymbol{\theta}_1)}{K_t(\boldsymbol{\theta})} \right) + \alpha_1 \right) \quad (35)$$

with final update rule

$$\boldsymbol{\theta}'_t = \boldsymbol{\theta} + \alpha_t G_\beta(\boldsymbol{\theta}) \quad (36)$$

where $\boldsymbol{\theta}'_t$ is the parameter for the PQC after one step of gradient ascent.

Variance of gradient

We now show how to calculate the variance of the gradient $\nabla K_t(\boldsymbol{\theta})$ using the Gaussian kernel. We assume a PQC with M parameters, QFIM $\mathcal{F}(\boldsymbol{\theta})$ and a target state $|\psi_t\rangle = \sqrt{K_0}|\psi(\boldsymbol{\theta}_t)\rangle + \sqrt{1-K_0}|\psi_0\rangle$, where $|\psi_0\rangle$ is some state that is orthogonal to any other state that can be represented by the PQC, i.e. $|\langle\psi_0|\psi(\boldsymbol{\theta})\rangle|^2 = 0 \forall \boldsymbol{\theta}$. The initial state of the PQC is $|\psi(\boldsymbol{\theta})\rangle$ with random parameter $\boldsymbol{\theta}$. We define the vector to the correct solution as $\Delta\boldsymbol{\theta} = \boldsymbol{\theta}_t - \boldsymbol{\theta}$. We now assume that the entries of the vector $\Delta\boldsymbol{\theta}$ are sampled from the uniform distribution $\Delta\boldsymbol{\theta}^{(n)} \sim \text{uniform}(-\sqrt{3}\frac{\sqrt{-4\log(A_0)}}{\sqrt{\text{Tr}(\mathcal{F})}}, \sqrt{3}\frac{\sqrt{-4\log(A_0)}}{\sqrt{\text{Tr}(\mathcal{F})}})$, where A_0 is identified later on. The mean is $\langle\Delta\boldsymbol{\theta}^{(n)}\rangle = 0$ and variance $\langle(\Delta\boldsymbol{\theta}^{(n)})^2\rangle = \frac{-4\log(A_0)}{\text{Tr}(\mathcal{F})}$. Further, the average of the product of index n and m of the parameter $\Delta\boldsymbol{\theta}$ is given by $\langle(\Delta\boldsymbol{\theta}^{(n)}\Delta\boldsymbol{\theta}^{(m)})\rangle = \delta_{nm}\frac{-4\log(A_0)}{\text{Tr}(\mathcal{F})}$, where δ_{nm} is the Kronecker delta. First, we calculate

$$\begin{aligned} \langle\Delta\boldsymbol{\theta}^T \mathcal{F} \Delta\boldsymbol{\theta}\rangle &= \sum_{n,m} \mathcal{F}_{nm} \langle\Delta\boldsymbol{\theta}^{(n)} \Delta\boldsymbol{\theta}^{(m)}\rangle \\ &= \sum_n \mathcal{F}_{nn} \langle\Delta\boldsymbol{\theta}^{(n)} \Delta\boldsymbol{\theta}^{(n)}\rangle = -4\log(A_0) \end{aligned}$$

Now, we assume that M is large, such that we can apply the central limit theorem $\langle e^{-\frac{1}{4}\Delta\boldsymbol{\theta}^T \mathcal{F} \Delta\boldsymbol{\theta}} \rangle \approx e^{-\frac{1}{4}\langle\Delta\boldsymbol{\theta}^T \mathcal{F} \Delta\boldsymbol{\theta}\rangle}$. Then, we find

$$A_0 = e^{-\frac{1}{4}\langle\Delta\boldsymbol{\theta}^T \mathcal{F} \Delta\boldsymbol{\theta}\rangle}. \quad (37)$$

We can now identify with the fidelity

$$K_t(\boldsymbol{\theta}) = K_0 e^{-\frac{1}{4}\langle\Delta\boldsymbol{\theta}^T \mathcal{F} \Delta\boldsymbol{\theta}\rangle} = A_0 K_0. \quad (38)$$

The gradient of the fidelity is given by

$$\nabla K_t(\boldsymbol{\theta}) = -\frac{1}{2} \mathcal{F} \Delta\boldsymbol{\theta} K_0 e^{-\frac{1}{4}\langle\Delta\boldsymbol{\theta}^T \mathcal{F} \Delta\boldsymbol{\theta}\rangle}. \quad (39)$$

We now want to calculate the variance of the n -th element of the gradient vector. The mean of the gradient $\langle\nabla K_t(\boldsymbol{\theta})\rangle = 0$. For the square of the gradient, we find

$$\langle(\nabla K_t(\boldsymbol{\theta})^{(n)})^2\rangle = \frac{1}{4} \langle((\mathcal{F} \Delta\boldsymbol{\theta})^{(n)})^2\rangle K_0^2 e^{-\frac{1}{8}\langle\Delta\boldsymbol{\theta}^T \mathcal{F} \Delta\boldsymbol{\theta}\rangle}. \quad (40)$$

We now calculate the element

$$\begin{aligned} \langle((\mathcal{F} \Delta\boldsymbol{\theta})^{(n)})^2\rangle &= \sum_{k,m} \langle\mathcal{F}_{nm} \Delta\boldsymbol{\theta}^{(m)} \mathcal{F}_{nk} \Delta\boldsymbol{\theta}^{(k)}\rangle \\ &= \sum_m \mathcal{F}_{nm} \mathcal{F}_{nm} \langle(\Delta\boldsymbol{\theta}^{(m)})^2\rangle = \sum_m \mathcal{F}_{nm} \mathcal{F}_{mn} \frac{-4\log(A_0)}{\text{Tr}(\mathcal{F})} \\ &= \frac{-4\log(A_0) (\mathcal{F}^2)_{nn}}{\text{Tr}(\mathcal{F})} \end{aligned}$$

where we used $\mathcal{F}_{mn} = \mathcal{F}_{nm}$ and $\sum_m \mathcal{F}_{nm} \mathcal{F}_{nm} = \sum_m \mathcal{F}_{nm} \mathcal{F}_{mn} = (\mathcal{F}^2)_{nn}$. Now, we take the average over the variance of the different gradient entries n and use the Pythagorean theorem (i.e. one can sum over the variance of independent variables)

$$\begin{aligned} \langle\langle(\mathcal{F} \Delta\boldsymbol{\theta})^{(n)}\rangle\rangle_{\Delta\boldsymbol{\theta}} &= \frac{1}{M} \sum_n \langle\langle(\mathcal{F} \Delta\boldsymbol{\theta})^{(n)}\rangle\rangle^2 \\ &= \frac{-4\log(A_0) \text{Tr}(\mathcal{F}^2)}{M \text{Tr}(\mathcal{F})}, \end{aligned}$$

where $\langle\langle.\rangle\rangle_{\Delta\boldsymbol{\theta}}$ indicates that we average first over $\Delta\boldsymbol{\theta}^{(n)}$ and then n . Finally, we get

$$\begin{aligned} \langle\langle(\nabla K_t(\Delta\boldsymbol{\theta})^{(n)})^2\rangle\rangle_{\Delta\boldsymbol{\theta}} &= -\log \left[\frac{K_t(\boldsymbol{\theta})}{K_0} \right] \frac{\text{Tr}(\mathcal{F}^2)}{M \text{Tr}(\mathcal{F})} K_0^2 e^{-\frac{1}{8}\langle\Delta\boldsymbol{\theta}^T \mathcal{F} \Delta\boldsymbol{\theta}\rangle} \\ &= \log \left[\frac{K_0}{K_t(\boldsymbol{\theta})} \right] K_t(\boldsymbol{\theta})^2 \frac{\text{Tr}(\mathcal{F}^2)}{M \text{Tr}(\mathcal{F})}. \end{aligned} \quad (41)$$

The variance becomes maximal when $K_t(\boldsymbol{\theta}) = K_0 \exp(-\frac{1}{2}) \approx 0.6K_0$. The variance of the gradient decays linearly with number of parameters M and is independent of qubit number N .

We now derive the lower bound of the variance. The variance of the eigenvalues of \mathcal{F} with M eigenvalues λ_n is always greater zero

$$\begin{aligned} \frac{1}{M} \sum_{n=1}^M \lambda_n^2 - \left(\frac{1}{M} \sum_{n=1}^M \lambda_n \right)^2 &\geq 0 \\ \sum_{n=1}^M \lambda_n^2 &\geq \frac{1}{M} \left(\sum_{n=1}^M \lambda_n \right)^2. \end{aligned}$$

With the relation $\text{Tr}(\mathcal{F}) = \sum_{n=1}^M \lambda_n$ and $\text{Tr}(\mathcal{F}^2) = \sum_{n=1}^M \lambda_n^2$, we find

$$\text{Tr}(\mathcal{F}^2) \geq \frac{1}{M} \text{Tr}(\mathcal{F})^2. \quad (42)$$

Thus, the variance is lower bounded by

$$\text{var}(\partial_k K_t(\boldsymbol{\theta})) \geq \frac{\text{Tr}(\mathcal{F}(\boldsymbol{\theta}))}{M^2} K_t(\boldsymbol{\theta})^2 \log \left[\frac{K_0}{K_t(\boldsymbol{\theta})} \right]. \quad (43)$$

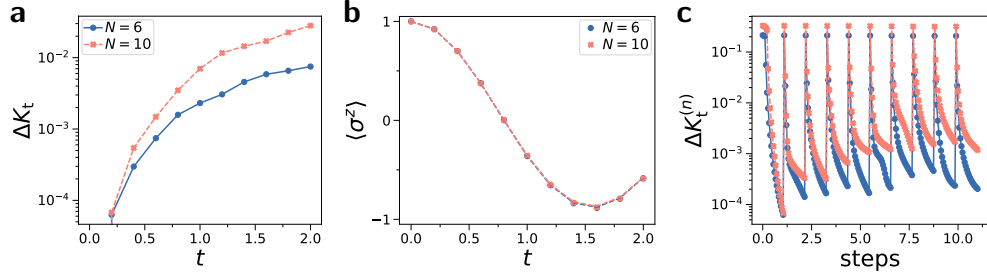


FIG. 14. Demonstration of projected variational quantum dynamics using adaptive gradient descent with GQNG ($\beta = \frac{1}{2}$). **a**) Fidelity in respect to the exact solution. **b**) Magnetization found compared to exact solution in dashed lines **c**) training loss for each Trotter step N_s , each trained with N_t training iterations. We simulate the evolution for total time $T = N_s \Delta t$ using $N_s = 10$ Trotter steps and $\Delta t = 0.2$, with each step trained with $N_t = 20$ training steps. The PQC used is YZ-CNOT with $p = N$, $J = 0.25$, $h = 1$ and initial state is the computational basis state with all zeros.

Fidelity of time evolution

Here, we show the lower bound of the fidelity of a time evolved state. Assume we evolve the state $|\psi\rangle$ with the Hamiltonian H for a time Δt . The eigenstates of H are given by $|\phi_n\rangle$ and eigenenergies by λ_n . The initial state is now expressed in terms of the eigenstates $|\psi\rangle = \sum_n \beta_n |\phi_n\rangle$, with overlap β_n with the n -th eigenstate. We assume that $|\psi\rangle$ has only non-zero overlap $\beta_n \neq 0$ with L eigenstates, where λ_1 is the smallest and λ_L the largest eigenvalue with non-zero overlap. We define $\Delta E = \lambda_L - \lambda_1$. Now, the evolved state is given by $|\psi'\rangle = \exp(-iH\Delta t)|\psi\rangle = \sum_{n=1}^L \beta_n e^{-i\lambda_n \Delta t} |\phi_n\rangle$. The fidelity between initial and evolved state is given by

$$K = |\langle \psi' | \psi \rangle|^2 = \left| \sum_{n=1}^L \beta_n^2 e^{-i\lambda_n \Delta t} \right|^2 = \quad (44)$$

We now derive a lower bound for K for small times Δt . K is minimal for small Δt when $|\beta_1|^2 = \frac{1}{2}$ and $|\beta_L|^2 = \frac{1}{2}$. This is evident as the relative phase between largest and smallest eigenvalues evolves the fastest. We have in this case

$$K = \frac{1}{2} (1 + \cos((\lambda_L - \lambda_1) \Delta t)) = \cos^2\left(\frac{\Delta E \Delta t}{2}\right). \quad (45)$$

Now, a lower bound for K can be found via a first order Taylor expansion

$$K > 1 - \frac{1}{4} (\Delta E \Delta t)^2. \quad (46)$$

Projected variational quantum dynamics

Here, we simulate the dynamics of the transverse Ising model with the projected variational quantum dynamics method [26]. The Hamiltonian is given by

$$H = J \sum_{n=1}^N \sigma_n^z \sigma_{n+1}^z + h \sum_{i=1}^N \sigma_i^x \quad (47)$$

In Fig.14a, we show the fidelity in respect to the exact solution. In Fig.14b, we show the dynamics of the magnetization $\langle \sigma^z \rangle = \langle \frac{1}{N} \sum_i \sigma_i^z \rangle$ over time t . We observe good match between simulation and exact result. In Fig.14c, we show the training loss for each of the Trotter steps.